Powder Technology 301 (2016) 412–420

Contents lists available at ScienceDirect

Powder Technology

journal homepage: www.elsevier.com/locate/powtec

Agglomeration process of surfactant-dispersed carbon nanotubes in unstable dispersion: A two-stage agglomeration model and experimental evidence

Shu Jian Chen [a], Cheng Yu Qiu [a], Asghar H. Korayem [b,c], Mohammad R. Barati [a], Wen Hui Duan [a,*]

[a] Department of Civil Engineering, Monash University, Clayton, VIC 3800, Australia
[b] Department of Civil Engineering, Iran University of Science and Technology, Narmak, Tehran 1684613114, Iran
[c] Department of Material Engineering, Monash University, Clayton, VIC 3800, Australia

ARTICLE INFO

Article history:
Received 5 February 2016
Received in revised form 19 May 2016
Accepted 17 June 2016
Available online 18 June 2016

Keywords:
Carbon nanotube
Dispersion
Agglomeration
UV–vis
Hydrodynamic size
Molecular dynamics

ABSTRACT

Dispersion of carbon nanotubes (CNTs) is key in the fabrication of CNT composites. Unstable dispersion of CNTs in matrix with Ca^{2+} and high alkalinity (pH > 12) hinders the development of CNT composites in the matrix. This study addresses this issue by advancing understanding of the agglomeration process of CNT via a new agglomeration model and experimental evidence. Naphthalene (NC) and lignosulfonate (SL) based surfactants are used to disperse CNTs in saturated $Ca(OH)_2$ solution. A continuous drop (over 50%) in the degree of dispersion is observed over 24 h. The model and experimental results suggest that there are two stages in this agglomeration process. The first stage is the formation of small CNT bundles with hydrodynamic size 710–950 nm, within 1 h after ultrasonication. Individual CNTs with hydrodynamic size 190–220 nm mostly disappear during this stage. The second stage is the formation of large 3D meshes (>4140 nm) by these CNT bundles. These small bundles can remain suspended for 2.5 h. The results show that the preferred number of CNTs in these bundles is 2–3 and 3–6 for SL and NC, respectively. This study suggests that dispersion of small CNT bundles is more stable than individual tubes and the degree of dispersion should be considered a time-sensitive parameter.

1. Introduction

Carbon nanotubes (CNTs) [1] play an important role in enhancing composite materials [2] due to their fiber-like geometry and superior engineering properties. In terms of reinforcement, CNTs possess the highest Young's modulus and strength of all known fibers [3,4] and are widely used in reinforcing polymer [5], metal [6–10] and ceramic [11] and cementitious material [12]. The small size of CNTs allows them to arrest cracking [13,14] in the composite from the nanometer-scale [12]. In addition, CNTs have been used to produce nanofluid and composites with high thermal [15–18] and electrical conductivity [9].

The dispersion of CNTs is key in the fabrication of these composite materials [19] and nanofluids. For their properties to be fully utilized, CNTs must be distributed in the matrix as individual tubes (or small bundles) [20]. Unfortunately, however, due to the strong van der Waals attraction between CNTs [21], they tend to agglomerate, especially in aqueous based solutions. To separate CNTs from agglomerates, high energy agitation such as ultrasonication and high shear [22] are often required. To improve the stability of the dispersion after separation, the surface of CNTs is often covalently modified or functionalized with non-covalently attached surfactants [23–25]. Non-covalent functionalization is preferred in many applications due to the superior integrity of the outer CNT walls [26].

In contrast to the dispersion of CNTs in organic solutions [27,28] and near neutral aqueous media [23], it is difficult to achieve a stable CNT dispersion in strong Ca^{2+} based alkaline media where the CNTs tend to agglomerate at a measurable rate. Studies have demonstrated that surfactant-dispersed CNTs can be colloidally stable in water without significant agglomeration for weeks [29]. In contrast, the performance of some effective surfactants such as sodium dodecyl sulfate (SDS) and sodium dodecylbenzenesulfonate (SDBS) deteriorates with elevated pH value [30,31]. In addition, divalent ions, such as Ca^{2+}, have been shown to promote graphene and CNTs to crosslink and form densely aggregated bulky papers [32]. The high valence of the counter ions promotes aggregation as suggested by the Schulze-Hardy rule [33].

Our limited understanding of the agglomeration process and morphology of CNTs hinders their application in alkaline environments with unstable dispersion, such as in clay and soil [34], cementitious material [35], and ceramic [11] based composites. With unstable CNT dispersion it is important to understand the size and morphology of the CNT agglomeration and its formation process. For example, it is critical to know whether CNTs form small, non-compact or large, compact agglomerates, because small agglomerates of CNTs containing a few

* Corresponding author.

http://dx.doi.org/10.1016/j.powtec.2016.06.033
0032-5910/

tubes can still be effective in terms of reinforcing effect [36] whereas large agglomerates need to be avoided in most applications [12]. Few studies of CNT dispersion in water involving highly alkaline (pH > 12) and Ca^{2+} based environment have been published. In the authors' previous work [37], the adsorption and distribution of CNTs in fresh cement paste were investigated and it is proposed that the agglomeration of process CNTs in thermodynamically unstable dispersion requires further research. It is vital, therefore, to improve our understanding of the behavior of CNTs in these unstable dispersions.

The present work experimentally investigates the agglomeration process and morphology of surfactant-dispersed CNTs in Ca^{2+} based strong alkaline solution and a new theoretical agglomeration model is proposed. Multi-walled CNTs (MWCNTs) are dispersed in saturated $Ca(OH)_2$ solution using naphthalene and lignosulfonate-based surfactants. These surfactants are known to disperse single-walled CNTs (SWCNTs) [38] and MWCNTs [39] better than common surfactants such as SDS and SDBS in that medium. The stability of the dispersion is studied and the morphology of the agglomerates is investigated. To improve understanding of the agglomeration process and morphology, a theoretical model is proposed to identify thermodynamic preferences during CNT agglomeration.

In order to estimate the interactions between surfactant, solution, and CNTs at nanometer level, which will provide the insight for the proposed agglomeration model, Molecular dynamics simulation is used in this study. MD simulation has been widely used to study the interaction between various surfactants and CNTs [40,41]. In the authors' previous work, MD simulations were used to calculate the interaction energy between CNT and SDS surfactant [42]. In this work, the self-energy [43] of CNTs wrapped by surfactants and the interaction energy between CNTs are estimated and combined with the proposed theoretical model to predict the preferred agglomeration process and morphology.

2. Experimental

2.1. Materials

The MWCNTs used in this study was purchased from Shenzhen Nanotech Port Co. Ltd. (Shenzhen, China). The properties of the MWCNTs are shown in Table 1. Naphthalene-sulfonic acid/formaldehyde calcium salt (CAS: 37293-74-6) based (NC) surfactant and Modified Sodium lignosulfonate based (SL) from BASF (Rheobuild®716LR) and Grace (WRDA®) and are used to assist the dispersion of the CNTs [44]. These surfactants have been proven to have adequate dispersion capabilities of CNTs in water [44].

2.1.1. Dispersion of CNTs in alkaline solutions

MWCNT and surfactants were added into the alkaline aqueous solution (saturated $Ca(OH)_2$) and sonicated with a 100 W ultrasonicator with a 5″ tip operating at 25% intensity. The total volume of each sample was 20 mL and the sonication time was 10 min (the corresponding input ultrasonication energy was around 750 J/mL). A water bath was used to keep the solution cool during ultrasonication. The concentration of the CNT adopted was 0.1 wt.% and 0.5 wt.% of surfactant was used. The surfactant to CNT mass ratio was 5 [45]. The pH value of the solutions was tested after sonication using a pH meter. The pH values of the solutions were 12.82 (±0.04) for SL and 12.69 (±0.03) for NC.

Table 1
Properties of the multi-walled CNTs.

Nominal outer diameter	Length	Purity	Specific surface area
10–20 nm	5–15 μm	>97%	90–120 m^2/g

2.1.2. UV–vis and TEM characterization

The sampled MWCNT suspensions and reference solutions were diluted by a factor of 100 and then analyzed using a HACH® DR5000 UV–vis spectrometer. To estimate the degree of dispersion, the range of the specific extinction coefficient at 500 nm was taken from the literature as 41.14 to 46.00 [37]. To observe the morphology of CNT bundles during CNT agglomeration, transmission electron microscopy was utilized. To prepare TEM samples, a droplet of the NC-CNT and SL-CNT suspension was pipetted onto a 400-mesh holey carbon-coated copper grid. After water evaporation, the samples were examined using a JEOL 2100F FEG TEM electron microscope operated at an accelerating voltage of 200 kV. TEM images of CNTs in large agglomerates were randomly taken in an area near the center of the TEM grid. Around 15 images were taken and >370 MWCNT bundles were measured for each sample using a grid-based method.

2.1.3. Zeta potential and hydro dynamic size

To determine the hydrodynamic size and the zeta potential of CNTs in suspensions, a ZetaSizer Nano ZS (Malvern Instruments Ltd., UK) instrument that uses dynamic light scattering was used. All CNT suspensions were equilibrated at a temperature of 25 °C for 2 min before measurements. The size measurement range was adjusted from 3 nm to 6000 nm. To check the reproducibility of the hydrodynamic size and zeta potential values, three sets of measurements were taken for each sample and the mean of the three experiments and resultant standard deviation were then reported.

3. MD simulation details

Molecular dynamics simulation was conducted using Materials Studio 5.5. COMPASS force field was used with an atom-based simulation method for van der Waals (vdW) force (cut-off distance: 9.5 Å) and Ewald Summation method (Ewald accuracy: 0.1 kcal/mol) for electrostatic forces. The interaction between the CNTs and the surfactants is predominantly vdW interactions Fig. 1 shows the molecular structures of the surfactants used in the simulation.

To obtain the interaction between CNTs and surfactant in solution, two cases were simulated where NCs and a SL containing 5 repeat units were attached to a (100, 100) triple-walled CNT surface (Fig. 9). The (100, 100) CNT, with outer diameter of 13.56 nm, was chosen to represent an intermediate value of the actual CNT diameter (10–20 nm). We simulated a section of the tube consisting of 10 aromatic rings in the circumferential direction which could be treated as a representative element to derive I_s for the entire tube.

The simulation comprised two steps. In the first step, conducted before the packing of solution molecules, the initial configurations of the CNT-surfactant complex were generated using the following procedures. First, a set of infinite graphene network was built that spanned over a periodic simulation box. This graphene network contained 3 layers, each of which was a section (1/10) of a (100,100) SWCNT (Fig. 9). The three layer of walls, with thickness of 10.23 Å, was found sufficient to capture most the MWCNT-surfactant interaction since the vdW interaction forces become insignificant beyond 10 Å. The size of the simulation box was 21.2 × 200 × 24.6 Å box with center symmetric configuration in the 200 Å directions. The length of the CNT is continuous in the periodic simulation box representing very long tubes. Then the surfactants were placed in a radially symmetric pattern around the CNTs with the hydrophilic groups facing outwards.

For NC and SL, parallel aggregation was used, allowing the hydrophilic groups to make contact with the solution. The surface densities, that is, the number of surfactants attached per nm^2 CNT surface, were gradually increased and the forces in the system were minimized. The interaction energy between the CNT and surfactants was calculated. This interaction energy increases with the surface density until it reached a threshold where adding more surfactants would overcrowd the surface and result in decreased interaction energy. We considered

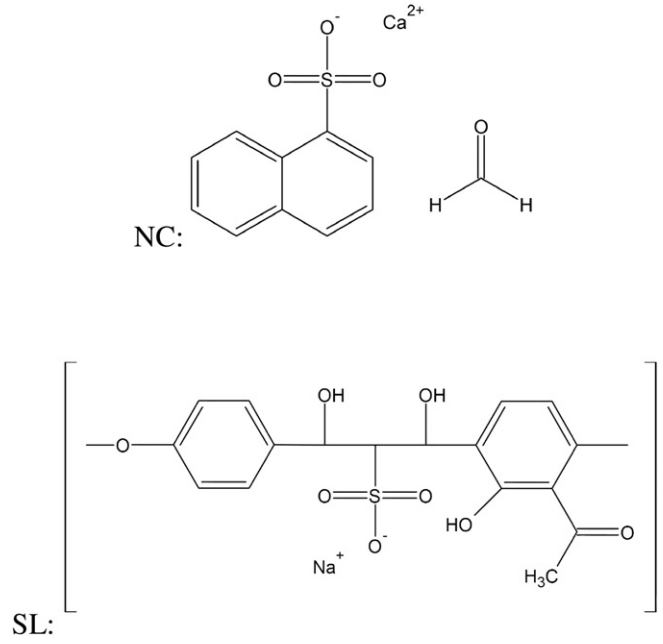

Fig. 1. Molecular structures of the surfactants used in the simulation. [47,61].

the surface density at this point as the starting point for the next step. This approximate saturation surface density may be slightly higher in MD due to the thermal oscillation and the solvent effect. However, such configurations allowed the system to reach saturation state easily in the MD simulation.

The second step began with packing the space with water, Ca^{2+}, and OH^- to make the pH value approximately equal to 12.5 and the density around 1 g/mL. For the NC, formaldehyde was also packed into the space. Geometry minimization was then conducted, followed by a 90 ps (canonical ensemble) NVT within which the self-energy of the CNT was stabilized. Then the structures were saved every 0.5 ps in successive 10 ps NVT for analysis. The interaction energy between the CNT surface and all surrounding molecules was calculated using the method detailed in the authors' previous publication [42]. The average interaction energy was calculated for the analysis period and used for the discussion.

Simulation was also conducted to calculate the CNT-CNT interaction energy for the (100,100) triple-walled CNTs. Two (100,100) triple-walled CNTs were built in free space, intersecting at their middle length with a minimum atom-to-atom distance of 0.34 nm. The interaction energy between these two tubes was also calculated using the method detailed in the authors' previous publication [42]. The interaction energy for five different intersecting angles (0, 22.5, 45, 67.5 and 90°) was computed, where 90° corresponds to the case where the two tubes are perpendicular.

4. Experimental investigation of CNT agglomeration

4.1. Stability of dispersion

The degree of dispersion of CNTs in NC-CNT and SL-CNT suspensions was obtained from UV–vis absorbance measurement and is shown in Fig. 2. The results show that a high degree of dispersion (80%) can be achieved after ultrasonication. Within 24 h, however, the degree of dispersion for both surfactants drops to below 30%. Both suspensions show the sharpest drop in degree of dispersion within 1 h, especially NC where this drop is over 50%. Generally, the results indicate that SL has higher absorbance and better dispersion efficacy under such conditions. When compared with CNT dispersions at lower pH (6–8), which can be

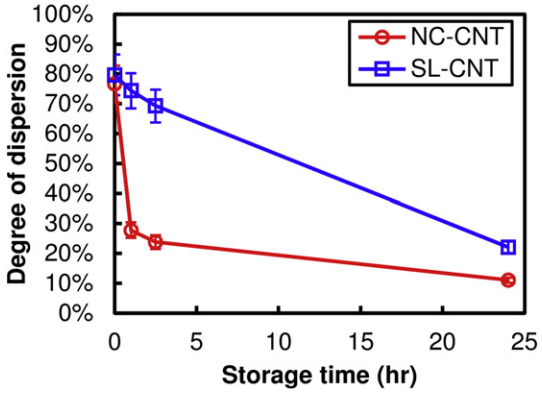

Fig. 2. Change in degree of dispersion for NC-CNT and SL-CNT suspensions over 24 h.

stable for weeks [45], the dispersion in $Ca(OH)_2$ induced high alkalinity is far less stable.

The zeta potentials of SL-CNT and NC-CNT solutions as a function of storage time were measured and are presented in Fig. 3. The changes in zeta-potential measurements indicate a two-stage process during CNT agglomeration. As shown in Fig. 3, immediately after ultrasonication the zeta potentials for both suspensions are nearly neutral, indicating negligible electrostatic repulsion between suspended particles, which implies rapid growth of the CNT agglomerates. Zeta potential close to zero has also been observed in surfactant dispersed particulate system at high pH (>10) [46]. After 1 h of storage the suspension enters the second stage, with zeta potentials of −11.7 and −16.3 mv for SL and NC, respectively. The suspended particles gain some mutual electrostatic repulsion during this stage, that may help slow the agglomeration process. From 1 h to 24 h, the electrostatic repulsion decreases due to further agglomeration of the CNTs. NC suspended CNTs are found to have more negative charges than SL suspended CNTs, due to the higher fraction of functional groups in NC [47]. It should be noted that the residual catalyst were reduced to a very low level during the purification process used in the production of CNTs [48,49] and high temperature (600–800 °C) is require to facilitate catalyst dissolution [50]. Therefore the behavior of the CNT dispersion is unlikely to be affected by the catalysts.

4.2. Bundle sizes of the dispersed MWCNTs

Fig. 4 shows the hydrodynamic size distribution of NC and SL-CNT suspensions after different storage times. Immediately after ultrasonication treatment, a single narrow peak with uniform hydrodynamic-sized CNT particles is observed for both surfactants. It can be seen that this single narrow peak of suspended CNTs is distinct with the board peak of the surfactant micelles (Fig. 4, NC and SL-no CNT). From

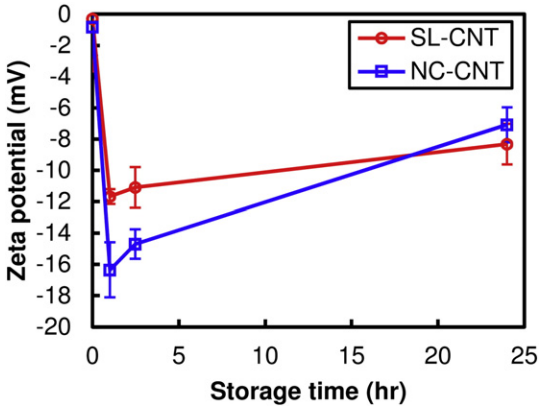

Fig. 3. Zeta potential of SL-CNT and NC-CNT suspensions as a function of storage time.

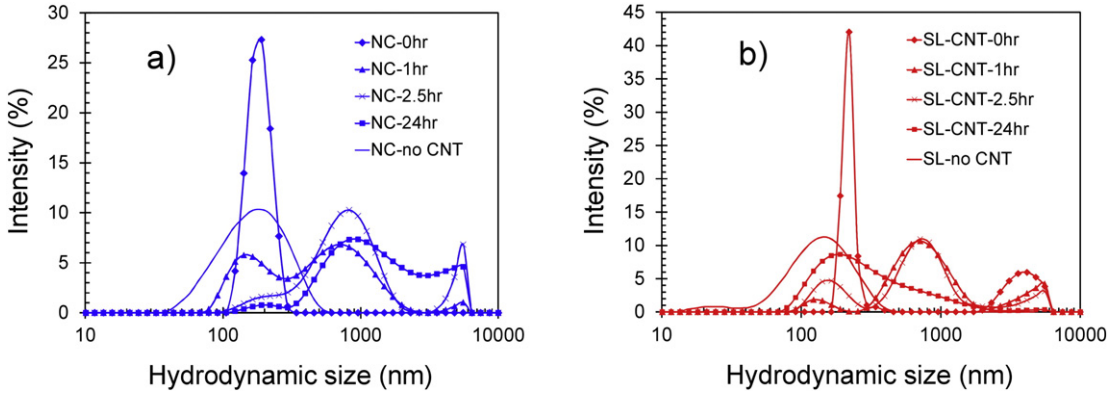

Fig. 4. The average hydrodynamic size distribution of CNTs in (a) NC-CNT and (b) SL-CNT solutions as a function of storage time. NC and SL –no CNT indicates the measurement of surfactants micelles in $Ca(OH)_2$ without the presence of CNTs.

1 h onwards, the distributions begin to show peak broadening as well as peak splitting, indicating the progressive agglomeration of CNTs.

As a result of the peak splitting, the distributions in Fig. 4 contain three different peaks, whose positions are presented in Table 2. Table 2 demonstrates that the positions of the three peaks are within similar ranges for the two surfactants: the first peak at around 120 nm–200 nm, the second peak at around 700 nm to 900 nm and the third peak at size >4000 nm. It can be identified that the third peak corresponds to the large CNT agglomerates and it often extends outside the measurable range of the equipment (5560 nm).

It is suggested that the first two peaks correspond to surfactant-dispersed CNTs about 100 nm to 1000 nm in hydrodynamic size [51]. The initial narrow, strong peak likely corresponds to the individually dispersed CNTs which mostly disappear within 2.5 h for both surfactants. By using the hydrodynamic model in Ref [52], the corresponding length and diameter of a CNT with hydrodynamic size 100–300 nm are found to be 300–1500 nm and 10–20 nm respectively which agree with the nominal dimension of CNTs given in Table 1. By comparing with the size distribution of the SL micelles (Fig. 4), it is suggested that the increase of a broad peak at 150–200 nm for SL from 2.5 to 24 h is due to the formation of SL micelles. More SL micelles are formed after more SL is released from CNTs as the CNT agglomerates. The second peak begins to become prominent after 1 h as a result of the bundling of the individual CNTs, but starts to decrease from 2.5 h to 24 h due to the further bundling of CNTs to form large agglomerates (peak 3). More detailed discussion of this process is presented subsequently together with the proposed model.

Fig. 5 shows two examples of transmission electron microscopies (TEM) images used to quantify the bundle size of the MWCNTs in NC and SL suspensions. A quantitative measurement scheme is adopted here to measure the CNT bundle sizes for both surfactant suspensions. The term 'bundle size' used here refers to the number of CNTs that is bundled together in a nearly parallel fashion.

Some examples of the measurement (red lines and numbers) are demonstrated in Fig. 5. This grid-based measurement method is performed in the following manner. Horizontal lines and vertical grid lines with a spacing of 200 nm are drawn across the TEM images. CNT and CNT bundles intersecting each line at an angle >45° are identified (demonstrated between the red lines in Fig. 5) and the number of tubes in each bundle (N) is measured and recorded (shown as numbers in Fig. 5). CNTs that are attached and align in a near parallel (~ ±15°) way are counted as a bundle. Counting bundles with intersection angles >45° avoids repeated measurements of bundles that intersect both horizontal and vertical grid lines. The intersection angle is defined as 0 when the bundle is parallel to the grid line and 90 when the bundle is perpendicular to the grid line. The proposed grid based method is used to estimate the probability of a statistical event where a CNT intersects a grid line with N-1 attached and aligned CNTs. The measurements are done in a zoomed in view of high resolution TEM images to minimize the error.

Fig. 6 shows the distribution of bundle size in each surfactant. It can be seen that the NC suspensions contain CNTs with generally larger bundle size than in the SL suspensions. In terms of the proportion of CNTs with different bundle sizes, it can be seen that the NC suspensions have a broader distribution than the SL suspensions. 53% of the CNTs in the SL suspensions have a bundle size smaller than 2 CNTs, compared to only 30% of the CNTs in the NC suspensions. On the other hand, the NC suspensions have around 20% of bundles with size >4 CNTs, whereas a negligible amount of the CNTs in the SL suspensions are in such large bundles. It should also be noted that almost no bundles observed for either suspension contain >7 CNTs.

Table 2
Average hydrodynamic size (H_D) CNTs in the NC-CNT and SL-CNT suspensions as a function of storage time.

	H_D (nm) at Peak 1	H_D (nm) at Peak 2	H_D (nm) at Peak 3
NC			
0 h	190.1 ± (12.3)[a]	–	–
1 h	141.7 ± (0.5)	712.3 ± (0.1)	5559.6 ± (0.3)
2.5 h	164.0 ± (0.5)	824.9 ± (2.9)	5559.6 ± (3.0)
24 h	220.1 ± (1.3)	955.4 ± (0.2)	5559.6 ± (0.7)
SL-CNT			
0 h	220.1 ± (36.4)	–	4145.4 ± (10.3)
1 h	122.42 ± (0.1)	712.3 ± (1.8)	5559.6 ± (1.0)
2.5 h	164.1 ± (3.3)	712.3 ± (4.2)	5559.6 ± (4.3)
24 h	190.1 ± (0.9)	–	–

[a] Numbers in bracket represent the standard deviation value.

5. Theoretical model of CNTs agglomeration

5.1. Parallel bundling of CNTs

Fig. 7-a illustrates an idealized model that presents one possible way for a CNT parallel bundle to increase in size. Oxygen containing functional groups, introduced during purification and functionalization [48,53], improves the affinities and dispersion of the CNTs with water but some charged groups (e.g. –COO–) repel the charged surfactants from attaching to the CNT surface. The CNTs used in this study (without functionalization treatment) showed rapid agglomeration in water without surfactants, indicating minimal amount of surface functional groups. Therefore, here the CNT surfactant interaction is considered as the main factor affecting the dispersion stability. In this idealized model, it is assumed that whenever only one tube is added to the bundle, all tubes are parallel and have identical diameter and length. The

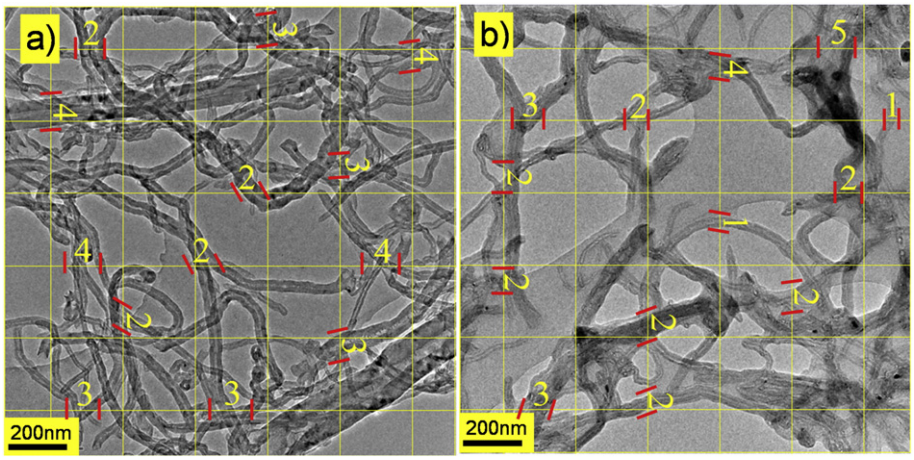

Fig. 5. TEM images of CNT agglomerates in NC-CNT (a) and SL-CNT (b) suspensions and examples of measurement of the bundle sizes of CNTs intersecting the grid. The measurements are shown as yellow numbers between two red lines that indicate the boundary of the bundle. For clarity, only a few measurements are shown.

central tube (tube 1 in Fig. 7-a) first attracts another 6 tubes to form the first shell layer surrounding itself (tube 2–7), then the second shell layer with 12 tubes (tube 8–19) is formed, and so on. With this defined order of growth, the surface area of the bundle is kept at a minimum. The average self-energy of individual tubes in a parallel bundle μ_N equals the sum of self-energy (of all the tubes in the bundle), S, divided by the number of tubes in that bundle, N [54].

When a single CNT attaches to an existing CNT bundle there are only three possible situations, as shown in Fig. 7-c to e. The changes in the sum of self-energy ΔS are different for these three situations and are given as

$$\Delta S = 2I_t + I_s, \text{situation 1} \tag{1}$$

$$\Delta S = 4I_t + \frac{1}{2}I_s, \text{situation 2} \tag{2}$$

$$\Delta S = 6I_t - I_s, \text{situation 3} \tag{3}$$

where I_t is the interaction energy between two CNTs, I_s is the interaction energy between an individually dispersed CNT and the surrounding surfactants and solution (Fig. 7-b).

The situations are demonstrated in Fig. 7-c to e. In situation 1, where one CNT is attached to another, one pair of tube-tube interactions ($2I_t$) is introduced and the surface area of the bundle that is in contact with solution is increased by the surface area of a whole tube (I_s). Since the contact area is relatively small for MWCNTs with a diameter beyond 10 nm, tube-solution interaction energy loss at the tube-tube contact point is not considered here.

When a tube attaches to two tubes, as in situation 2, two pairs of tube-tube interactions are introduced resulting in a $4I_t$ increment in S. The attached tube leads to one sixth of the surface area of each tube being isolated from the solution (blue dashes in Fig. 7-d). Thus, the net increment in contact area with solution is half of a whole tube and the corresponding ΔS is $\frac{1}{2}I_s - I_s$. Likewise, in the last situation where one tube attaches to three tubes, three pairs of tube-tubes interactions ($6I_t$) are added while the net increment in contact area with the solution is zero.

If a bundle grows in the order proposed in Fig. 7-a, for the M layer of shell containing $6M$ tubes, K is an integer used to index a tube in the shell layer. The shell grows in the sequence $K = 1$ to $6M$. Then, for $N = 2 \to \infty$ the corresponding situation for each added tube can be determined by the following rules:

$$\text{situation 1} : K = 1, M = 1 \tag{4}$$

$$\text{situation 2} : 2 < K < M, M = 1 \text{ or } K \bmod M = 1 \cap K \neq 1, M > 1 \text{ or } K = 2, M > 1 \tag{5}$$

$$\text{situation 3} : K = M, M = 1 \text{ or } K \bmod M \neq 1 \cup K = 1 \cap K \neq 2, M > 1. \tag{6}$$

5.2. Tangling of CNTs or CNT bundles

Here, another possible CNT agglomeration scheme is discussed, where CNTs or CNT bundles attach to each other in a non-parallel fashion. This type of aggregation, also widely reported in the literature, is often referred to as tangling of CNTs [55]. The real tangling morphology is very complex as the tubes are curved and intersect with each other in a range of angles.

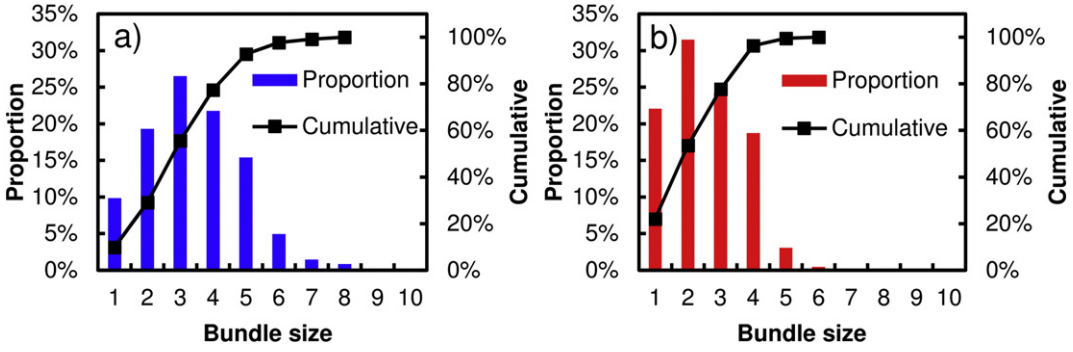

Fig. 6. Proportion of MWCNTs in bundles of different sizes in (a) NC and (b) SL suspension as measured from TEM images.

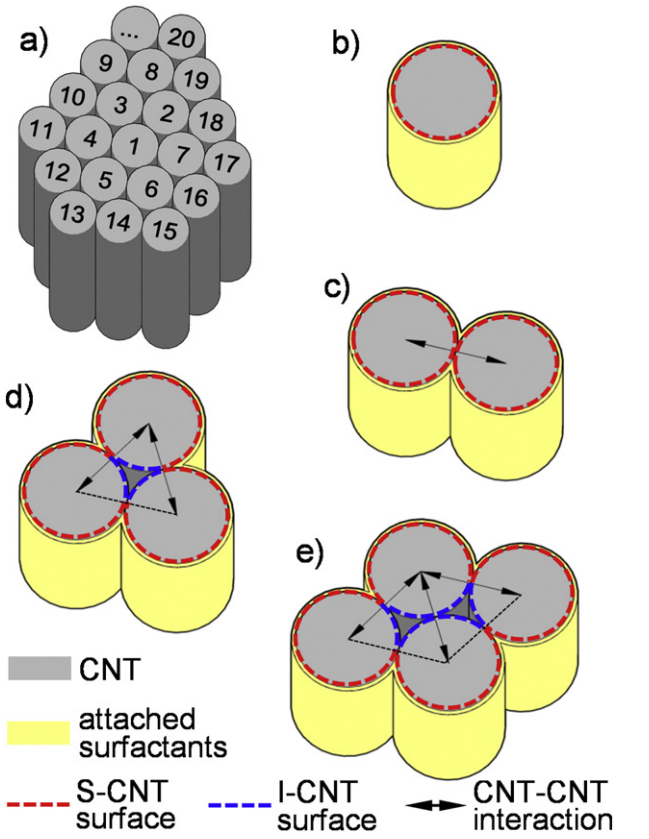

Fig. 7. Schematics of an idealized CNT bundle growth model. a) A growing CNT bundle with a hexagonal shape and CNTs attaching to the bundle following the sequence indicated by the numbers (1–20 …). b) A single tube in solution, c) Situation 1: a tube attaches to another tube. Arrows indicate the formation of tube-tube van der Waals interaction. d) Situation 2: a tube attaches to two bundled tubes. e) Situation 3: a tube attaches to three bundled tubes. Note. S-CNT surface: CNT surfaces in contact with surfactants and solution. I-CNT surface: CNT surfaces isolated from surfactants and solution.

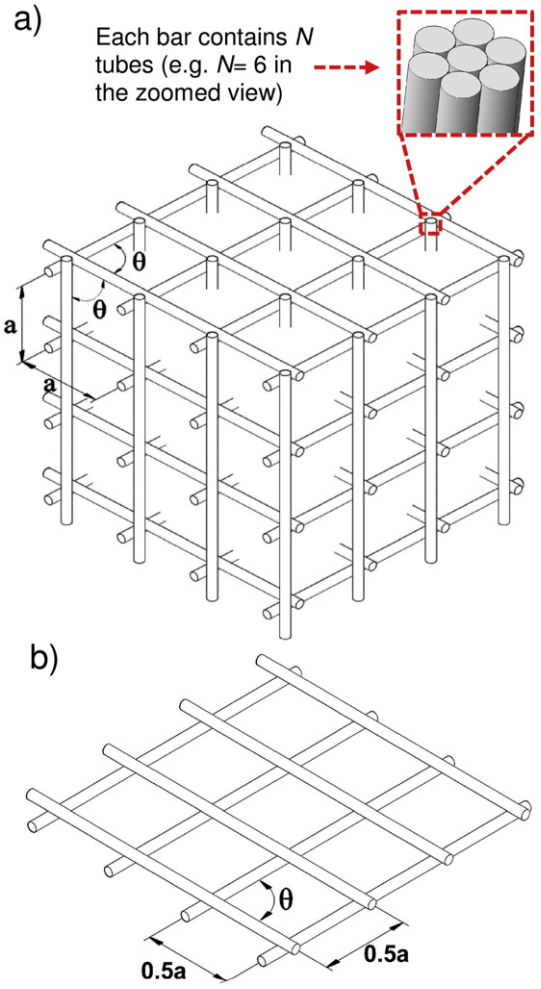

Fig. 8. 3D (a) and 2D (b) mesh models of a tangled CNT network. Every bar in the meshes represents a CNT bundle that contains one or more parallel CNTs.

To present the effect of tangling on the self-energy of CNTs, we propose a 3D mesh model as shown in Fig. 8-a. In Fig. 8, every bar can be regarded as a CNT or a bundle of parallel CNTs. The spacing of these bars (a) is used to represent the density of the agglomeration and a constant intersecting angle (θ) is assumed. For more intuitive demonstration and simplicity of calculation, this 3D mesh model can be equalized to a 2D mesh model (Fig. 8-b) where a is reduced to $0.5a$. Every bar in this 2D mesh has the same number of intersecting bars as in the 3D mesh. Moreover, this 2D mesh model can also represent the CNT agglomeration observed in TEM or scanning electron microscopy (SEM), where 3D agglomerations collapse into 2D meshes due to drying of the solution.

Using the 2D mesh model, if one bundle containing N CNTs intersects with n ($n = 2L/\alpha$) other bundles, each of which also contains N CNTs, the increase in S due to the intersections can be expressed as

$$S_t(x) = k\frac{nI_t'}{NL}, 2<n<\frac{2L\sin\theta}{d} \tag{7}$$

where $S_t(x)$ is the average self-energy due to tangling for a mesh of CNTs, L is the length of CNTs, d is the diameter of the CNTs, k is a coefficient describing the number of pairs of tube-tube interactions that are introduced at the bar-bar intersecting point (e.g. for a 19-tube hexagonal bundle, k varies between 1 and 3 since there are at most 3 tubes at one edge of the bundle), and I_t' is the angle dependent variants of I_t, x is the number of CNTs in an agglomerate ($x = N$ for pure parallel agglomerate while $x = 2nN$ or $x = \frac{3}{4}n^2N$ in an equivalent 3D mesh).

5.3. Estimation of I_s, I_t, and I'_t using MD simulations

I_s is obtained by MD simulation where the NC and SL-MWCNTs systems are simulated at atomic level. The snapshots in Fig. 9 provide views of the typical assembling morphology of the surfactants on the CNT surface. In both assemblies, the hydrophobic groups on the surfactants (e.g. methyl and phenyl groups) attach to the CNT surface whereas the hydrophilic groups (e.g. hydroxyl and sulfonic groups) face the solution. The repulsive force between the negatively charged hydrophilic groups resists the reagglomeration of the CNTs [56,57]. As shown in Fig. 9, the I_s of the NC-MWCNT system is 24% less negative than that of the SL-system.

I_t is calculated to be −107 kcal/mol/nm based on our MD simulation of a pair of (100,100) CNTs. For the MWCNT used in this study, the I_t' for different angles is computed using MD simulation and plotted in Fig. 10. It can be seen that the smaller the angle, the stronger the CNT-CNT interaction (indicated by a more negative I_t').

6. Understanding the agglomeration process

6.1. Energetically preferred agglomeration process

Based on the model and the values I_s, I_t, and I'_t obtained from the MD simulations, one can derive the average self-energy for tubes in different types of agglomerate (parallel bundled or tangled), which is shown in Fig. 11. Entropy increase in the CNT dispersion system can be caused

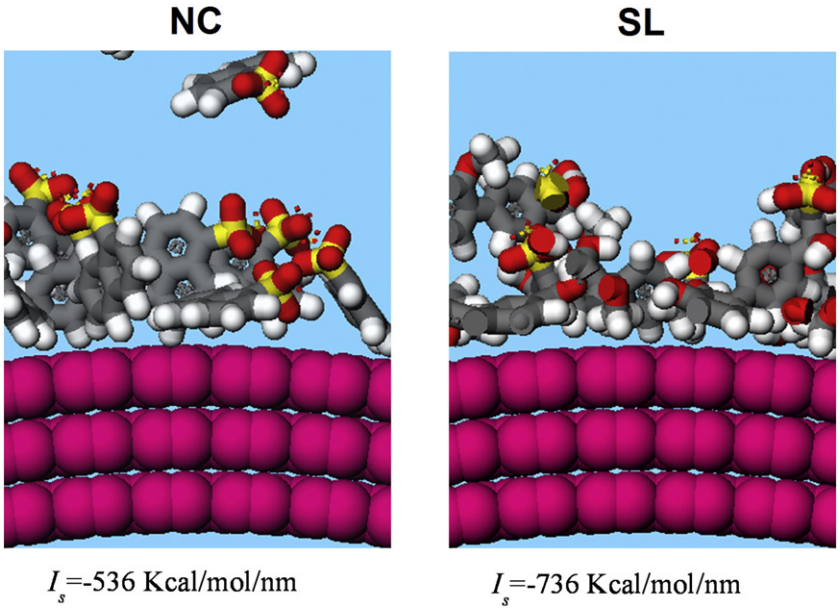

Fig. 9. Interaction energy per unit length of CNT and snapshots of NC (left) and SL chain (right) aggregations on a simulated (100, 100) triple-walled CNT surface. Red: oxygen; gray: carbon; white: hydrogen; yellow: sulfur; purple: CNT surface. Water and $Ca(OH)_2$ are rendered invisible for clarity.

by the reduced self-energy of the CNTs. Therefore, CNTs tend to move into a preferred state with more negative self-energy to increase the entropy. By estimating the self-energy of different states, the preferred agglomeration state can be identified.

In Fig. 11, the increase of x (number of CNTs in a CNT agglomerate) can be due to the increase of n or N. For example, when $n = 0$ and $N \geq 1$, increase of x is due to parallel bundling (increase of N); when $n \geq 0$ and $N = 2$ or 4, the increase of x is due to tangling (increase of n). In Eqs. (1)–(6), the average self-energy per tube for parallel bundled CNTs ($n = 0$, $N \geq 1$) can be calculated. As indicated in Fig. 11, for both suspension when $n = 0$ and N grows towards infinity, μ_x converges to the state of CNT solid ($\mu_{\infty,n=0}$ in Fig. 11) where each CNT is interacting with only 6 other CNTs as in its first shell layer. Based on the Boltzmann distribution, a more negative μ_x makes the formation of bundles of that particular size energetically preferable and increases their concentration in the solution [54]. The two preferred bundle sizes with the most negative μ_x are 6 and 5 ($x = N = 6$ or 5) for NC and 2 and 3 ($x = N = 2$ or 3) for SL. It is implied that these bundle sizes should be the dominant fraction in the respective CNT suspension.

When tangling agglomeration is taken into consideration with $n > 0$ (Eq. (7)), first, the effect of the intersecting angle is investigated. As shown in Fig. 11, the difference between the curves with $\theta = 22.5°$ ($\pi/8$) and 90° ($\pi/2$) is small for both NC and SL up to an agglomerate size of 2000. This indicates that as long as the tubes are not parallel bundled, the intersecting angle, θ, creates no significant changes in μ_x.

The magnitude of μ_x decreases when the size of parallel bundles increases beyond the preferred bundle size (6 and 3 for NC and SL respectively). If tangling of CNTs is considered, the magnitude of μ_x can continue to increase after the preferred bundle size is reached by forming 3D/2D meshes, as shown by the curves in Fig. 11 with $n > 0$. In such cases, every bar in the mesh models (Fig. 8) is a bundle of CNTs with the optimal bundle size and x is increased by increasing the number of bars within the meshes, causing the magnitude of μ_x to further increase due to more bar-bar intersections.

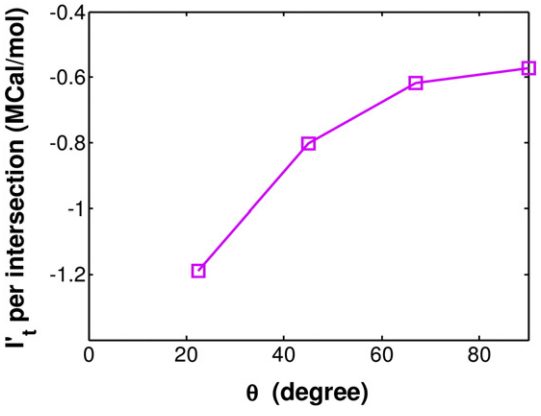

Fig. 10. Tube-tube interaction energy for MWCNT at different intersection angles.

6.2. Model-suggested agglomeration process and experimental evidence

The energetically preferred agglomeration process predicted by the proposed model for NC and SL is first parallel bundled (stage 1) before reaching the optimum bundle size and then tangling (stage 2) to form

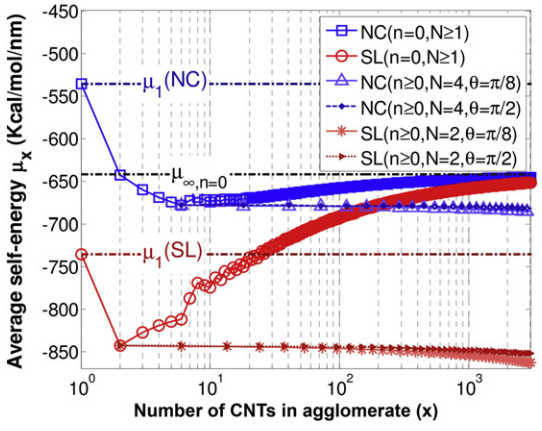

Fig. 11. Average self-energy μ_x per nm for different cases. The dashed lines represent the value of μ_x for individually dispersed CNTs (μ_1) and parallel bundles of infinite size ($\mu_{\infty,n=0}$). $k = 3$ and 2 for NC and SL respectively. The length and diameter of the CNTs are assumed to be 2 μm and 10 nm respectively.

Table 3
Suggested agglomeration process of CNTs and experimental evidence.

Experimental results in this study	Initial	Stage 1	Stage 2
(A) Suggested by the idealized theoretical model with MD simulation (Figs. 7, 11)	Single tubes	Parallel bundles Preferred bundle size: NC: 5.6 SL: 2.3	Meshes of bundles
(B) UV–vis results (Fig. 2)	80% degree of dispersion for both NC and SL	Decreasing rate of degree of dispersion: NC: 50%/h SL: 6%/h	Decreasing rate of degree of dispersion: NC: 0.7%/h SL: 2.2%/h
(C) Zeta potential measurements (Fig. 3)	Immediately after ultrasonication Zeta potential ≈ 0	Within 1 h small bundles form and Zeta potential decreases to NC: −16.3 mv SL: −11.7 mv	1–24 h, Zeta potential increases slowly due to the formation of large agglomerates
(D) Hydrodynamic size measurements (Fig. 4, Table 2)	Peak 1 (190–220 nm)	Peak 2 (710–950 nm)	Peak 3 (>4140 nm)
(E) TEM imaging and grid-based analysis (Figs. 5, 6)	–	Preferred bundle size: NC: 3.4 SL: 2.3 Bundle size limit (95% percentile): NC: 6 SL: 4	Mesh formed by the bundles
(F) Suggestions for real conditions	Dispersed tubes	Formation of small bundles of tubes	Formation of Large 3D (non-parallel) agglomerates

larger 3D agglomerations. The suggested agglomeration process is summarized in Table 3 and compared with experimental evidence.

The measurements of zeta potential (Table 3-C), hydrodynamic size (Table 3-D) and TEM (Table 3-E) agree with the energetically preferred 2-stage agglomeration process (Table 3-A). In terms of stage 1, the decrease in zeta potential (Table 3-C) and stabilization of the suspension during the first hour could be a result of the nearly parallel bundling of CNTs. As suggested in Fig. 11, the change from an individual tube to a parallel bundle with a few tubes (5–6 for SL and 2–3 for NC) dramatically decreases μ_x whereas forming 3d agglomerates of 2000 bundles only slightly decreases μ_x. Therefore, parallel bundling has the higher driving potential [54] and should occur more rapidly than 3D tangling. This is also shown in the hydrodynamic sizes (Table 3-D), where individual tubes (peak 1) mostly disappear in the first hour (Fig. 4, Table 2). Individual tubes are the least stable, as suggested by both zeta potential, hydrodynamic size, and the model. Therefore, stage 1 ends within a very short time (<1 h in these cases).

In stage 2, the suspension becomes metastable because μ_x reaches negative plateaus (curves with $n \geq 0$ in Fig. 11). The curves with $n \geq 0$ in Fig. 11 can be treated as plateaus since the decrease of μ_x is relatively small when x is smaller than 1000. $n \geq 0$ corresponds to the case where the CNT bundles tangle to form 3D agglomerates. Zeta potentials in the second stage increase gradually from 1 to 24 h. This increase is due to the detaching of surfactants from the surface of CNTs, increasing the ionic strength in bulk solution [58] and contracting the electrical double layer [59]. The hydrodynamic size measurement (Table 3-D) also shows that small bundles (peak 2) remain prominent until 2.5 h and gradually disappear from 2.5 to 24 h. TEM observation of bundle sizes (Table 3-D) is in good agreement with the energetically preferred bundle sizes suggested by the model (Table 3-D). Almost no bundle size >7 is observed in the experiment because further bundling increases μ_x. Bundles in NC-CNT suspensions are generally of larger size than those in SL-CNT suspensions in both TEM observation (Table 3-D) and the modeling results (Table 3-A).

The UV–vis absorbance results indicate a decrease in the degree of dispersion, reflecting the agglomeration process. In the first hour (stage 1), NC-CNT suspension show a much more significant decrease in the degree of dispersion than SL-CNT suspension (Table 3-B). This is likely due to the formation of the larger bundles in the NC-CNT suspension, as suggested by TEM and the model. In Table 3-B, both surfactants showed a lower rate of decrease in the degree of dispersion in stage two (after 1 h) than in stage 1. This is consistent with the point in the previous paragraph that the formation of larger large agglomerates progress occurs at a lower rate.

Due to imperfections in CNT geometry, more randomness can be seen in the agglomeration process and morphology in the real condition (Table 3-F) than in the idealized condition (Table 3-A). One should note that the model used here is an idealized model that does not consider variation in diameter, length defects, and curvatures of CNTs [12,36]. These variations prevent perfect bundle formation as shown in (Table 3-A). Therefore, more randomness is seen in the real agglomeration process as shown in Table 3-F, although the energetic preference to form small bundles and then large agglomerates still persists (as shown in the TEM observation in Table 3-D).

The results here provide some guidance for the fabrication and understanding of CNT composites involving Ca^{2+} based alkaline environments. The first indication is that CNTs should be treated as very small bundles rather than individual CNTs in these environments. The fabrication method and modeling should be modified accordingly to address this difference. Another indication is that the time-dependency of the dispersion should be noted in the fabrication of these composites. Methods such as rapid setting or hardening of the matrix material may help to achieve better dispersion of CNTs because the individual tubes and small bundles can be fixed in position to prevent further agglomeration.

7. Conclusions

Our UV–vis measurements show that the NC and SL facilitated dispersion of CNTs in a Ca^{2+} based alkaline environment shows a continuous decrease in the degree of dispersion after ultrasonication, with a 50% drop over 24 h. Zeta potential and hydrodynamic size indicate that there are two stages in the agglomerations process. A model is proposed to help explain these two stages by simulating the agglomeration of CNT under ideal conditions. The model suggests that the CNTs prefer to rapidly form small, nearly parallel bundles and then slowly grow into 3D mesh-like agglomerates. Moreover, experimental measurement shows that individual CNTs with the hydrodynamic size of 190–220 nm form bundles with the hydrodynamic size of 710–950 nm within 1 h. These small bundles gradually form larger agglomerates (hydrodynamic size >4140 nm) from 2.5 to 24 h after ultrasonication. The model also suggests that SL can maintain the CNT bundles at a smaller size (2–3 tubes per bundle) than NC (5–6 tubes per bundles). This conclusion is supported by TEM observation with preferred bundle sizes of 2–3 and 3–4 for SL and NC respectively. The unstable dispersion of CNT is still usable for CNT composites given that the CNTs are controlled in the form of small bundles.

Acknowledgments

The authors are grateful for the financial support of the Australian Research Council for conducting this study. The authors acknowledge the use of facilities within the Monash Centre for Electron Microscopy.

References

[1] M.F. Yu, O. Lourie, M.J. Dyer, K. Moloni, T.F. Kelly, R.S. Ruoff, Strength and breaking mechanism of multiwalled carbon nanotubes under tensile load, Science 287 (2000) 637–640.
[2] P.K. Mehta, P. Monteiro, Concrete: Structure, Properties, and Materials, Prentice Hall, 1993.
[3] M.-F. Yu, Fundamental mechanical properties of carbon nanotubes: current understanding and the related experimental studies, J. Eng. Mater. Technol. 126 (2004) 271–278.
[4] Q. Zhao, M.B. Nardelli, J. Bernholc, Ultimate strength of carbon nanotubes: a theoretical study, Phys. Rev. B. 65 (2002) 144105.
[5] A.H. Korayem, M.R. Barati, S.J. Chen, G.P. Simon, X.L. Zhao, W.H. Duan, Optimizing the degree of carbon nanotube dispersion in a solvent for producing reinforced epoxy matrices, Powder Technol. 284 (2015) 541–550.
[6] M.M. Sotoudehnia, A. Paúl, Dispersion of carbon nanotubes in iron by wet processing for the preparation of iron–carbon nanotube composites, Powder Technol. 258 (2014) 1–5.
[7] T. Peng, I. Chang, Uniformly dispersion of carbon nanotube in aluminum powders by wet shake-mixing approach, Powder Technol. 284 (2015) 32–39.
[8] F. Rikhtegar, S. Shabestari, H. Saghafian, The homogenizing of carbon nanotube dispersion in aluminium matrix nanocomposite using flake powder metallurgy and ball milling methods, Powder Technol. 280 (2015) 26–34.
[9] Y. Zhang, Q.-q. Yao, H.-l. Gao, L.-z. Wang, X.-l. Jia, A.-q. Zhang, Y.-h. Song, T.-c. Xia, H.-c. Dong, Facile synthesis and electrochemical performance of manganese dioxide doped by activated carbon, carbon nanofiber and carbon nanotube, Powder Technol. 262 (2014) 150–155.
[10] C. Hai, T. Shirai, M. Fuji, Fabrication of conductive porous alumina (CPA) structurally modified with carbon nanotubes (CNT), Adv. Powder Technol. 24 (2013) 824–828.
[11] K. Mohammad, N. Saheb, Molecular level mixing: an approach for synthesis of homogenous hybrid ceramic nanocomposite powders, Powder Technol. 291 (2016) 121–130.
[12] S. Chen, F. Collins, A. Macleod, Z. Pan, W. Duan, C. Wang, Carbon nanotube–cement composites: a retrospect, IES J. Part A Civil Struct. Eng. 4 (2011) 254–265.
[13] Z. Li, S.P. Shah, Localization of microcracking in concrete under uniaxial tension, ACI Mater. J. 91 (1994).
[14] Z. Li, Advanced Concrete Technology, John Wiley & Sons, 2011.
[15] R. Mondragón, C. Segarra, R. Martínez-Cuenca, J.E. Juliá, J.C. Jarque, Experimental characterization and modeling of thermophysical properties of nanofluids at high temperature conditions for heat transfer applications, Powder Technol. 249 (2013) 516–529.
[16] A. Yu, C. Feng, R. Zou, R. Yang, On the relationship between porosity and interparticle forces, Powder Technol. 130 (2003) 70–76.
[17] R. Sule, P. Olubambi, I. Sigalas, J. Asante, J. Garrett, Effect of SPS consolidation parameters on submicron Cu and Cu–CNT composites for thermal management, Powder Technol. 258 (2014) 198–205.
[18] L. Chen, W. Yu, H. Xie, Enhanced thermal conductivity of nanofluids containing Ag/MWNT composites, Powder Technol. 231 (2012) 18–20.
[19] M.B. Vishlaghi, A. Ataie, Investigation on solid solubility and physical properties of Cu–Fe/CNT nano-composite prepared via mechanical alloying route, Powder Technol. 268 (2014) 102–109.
[20] S.J. Chen, F.G. Collins, A.J.N. Macleod, Z. Pan, W.H. Duan, C.M. Wang, Carbon nanotube-cement composites: a retrospect, the IES journal part a: civil &amp, Struct. Eng. 4 (2011) 254–265.
[21] L.A. Girifalco, M. Hodak, R.S. Lee, Carbon nanotubes, buckyballs, ropes, and a universal graphitic potential, Phys. Rev. B 62 (2000) 13104–13110.
[22] G.-H. Xu, Q. Zhang, J.-Q. Huang, M.-Q. Zhao, W.-P. Zhou, F. Wei, A two-step shearing strategy to disperse long carbon nanotubes from vertically aligned multiwalled carbon nanotube arrays for transparent conductive films, Langmuir 26 (2009) 2798–2804.
[23] B. Munkhbayar, M.J. Nine, J. Jeoun, M. Bat-Erdene, H. Chung, H. Jeong, Influence of dry and wet ball milling on dispersion characteristics of the multi-walled carbon nanotubes in aqueous solution with and without surfactant, Powder Technol. 234 (2013) 132–140.
[24] N. Poorgholami-Bejarpasi, B. Sohrabi, Self-assembly of cationic surfactants on the carbon nanotube surface: insights from molecular dynamics simulations, J. Mol. Model. 19 (2013) 4319–4335.
[25] R.P. Singh, S. Jain, P. Ramarao, Surfactant-assisted dispersion of carbon nanotubes: mechanism of stabilization and biocompatibility of the surfactant, J. Nanoparticle Res. 15 (2013) 1–19.
[26] J.N. Coleman, U. Khan, W.J. Blau, Y.K. Gun'ko, Small but strong: a review of the mechanical properties of carbon nanotube-polymer composites, Carbon 44 (2006) 1624–1652.
[27] G. Pircheraghi, R. Foudazi, I. Manas-Zloczower, Characterization of carbon nanotube dispersion and filler network formation in melted polyol for nanocomposite materials, Powder Technol. 276 (2015) 222–231.
[28] X.-L. Jia, Q. Zhang, J.-Q. Huang, C. Zheng, W.-Z. Qian, F. Wei, The direct dispersion of granular agglomerated carbon nanotubes in bismaleimide by high pressure homogenization for the production of strong composites, Powder Technol. 217 (2012) 477–481.
[29] M.D. Tiwari, G.H. Sagar, J.R. Bellare, Flow cytometry-based evaluation and enrichment of multiwalled carbon nanotube dispersions, Langmuir 28 (2012) 4939–4947.
[30] V.C. Moore, M.S. Strano, E.H. Haroz, R.H. Hauge, R.E. Smalley, J. Schmidt, Y. Talmon, Individually suspended single-walled carbon nanotubes in various surfactants, Nano Lett. 3 (2003) 1379–1382.
[31] B. White, S. Banerjee, S. O'Brien, N.J. Turro, I.P. Herman, Zeta-potential measurements of surfactant-wrapped individual single-walled carbon nanotubes, J. Phys. Chem. C 111 (2007) 13684–13690.
[32] Y.-A. Li, N.-H. Tai, S.-K. Chen, T.-Y. Tsai, Enhancing the electrical conductivity of carbon-nanotube-based transparent conductive films using functionalized few-walled carbon nanotubes decorated with palladium nanoparticles as fillers, ACS Nano 5 (2011) 6500–6506.
[33] M. Sano, J. Okamura, S. Shinkai, Colloidal nature of single-walled carbon nanotubes in electrolyte solution: the Schulze–Hardy rule, Langmuir 17 (2001) 7172–7173.
[34] S. Martínez-Ramírez, M. Frias, Micro-Raman study of stable and metastable phases in metakaolin/Ca (OH)2 system cured at 60 °C, Appl. Clay Sci. 51 (2011) 283–286.
[35] Y.M. Tang, Y.F. Miao, Y. Zuo, G.D. Zhang, C.L. Wang, Corrosion behavior of steel in simulated concrete pore solutions treated with calcium silicate hydrates, Constr. Build. Mater. 30 (2012) 252–256.
[36] S.J. Chen, B. Zou, F. Collins, X.L. Zhao, M. Majumber, W.H. Duan, Predicting the influence of ultrasonication energy on the reinforcing efficiency of carbon nanotubes, Carbon 77 (2014) 1–10.
[37] S.J. Chen, W. Wang, K. Sagoe-Crentsil, F. Collins, X.L. Zhao, M. Majumder, W.H. Duan, Distribution of carbon nanotubes in fresh ordinary Portland cement pastes: understanding from a two-phase perspective, RSC Adv. (2015).
[38] J. Makar, The Effect of SWCNT and Other Nanomaterials on Cement Hydration and Reinforcement, Nanotechnology in Civil Infrastructure, Springer, Berlin; Heidelberg 2011, pp. 103–130.
[39] F. Collins, J. Lambert, W.H. Duan, The influences of admixtures on the dispersion, workability, and strength of carbon nanotube-OPC paste mixtures, cement &amp, Concr. *compos.* 34 (2012) 201–207.
[40] S.C. Lin, D. Blankschtein, Role of the bile salt surfactant sodium cholate in enhancing the aqueous dispersion stability of single-walled carbon nanotubes: a molecular dynamics simulation study, J. Phys. Chem. B 114 (2010) 15616–15625.
[41] Z.J. Xu, X.N. Yang, Z. Yang, A molecular simulation probing of structure and interaction for supramolecular sodium dodecyl sulfate/single-wall carbon nanotube assemblies, Nano Lett. 10 (2010) 985–991.
[42] W.H. Duan, Q. Wang, F. Collins, Dispersion of carbon nanotubes with SDS surfactants: a study from a binding energy perspective, Chem. Sci. 2 (2011) 1407–1413.
[43] J.N. Israelachvili, Intermolecular and Surface Forces, Academic Press, 2011.
[44] F. Collins, J. Lambert, W.H. Duan, The influences of admixtures on the dispersion, workability, and strength of carbon nanotube–OPC paste mixtures, Cem. Concr. Compos. 34 (2012) 201–207.
[45] J.R. Yu, N. Grossiord, C.E. Koning, J. Loos, Controlling the dispersion of multi-wall carbon nanotubes in aqueous surfactant solution, Carbon 45 (2007) 618–623.
[46] A. Kaya, Y. Yukselen, Zeta potential of soils with surfactants and its relevance to electrokinetic remediation, J. Hazard. Mater. 120 (2005) 119–126.
[47] ChemicalTradingGuide, Naphthalenesulfonic Acid, Polymer With Formaldehyde, Calcium Salt (CAS No. 37293-74-6), 2012.
[48] Q. Zhang, J.Q. Huang, W.Z. Qian, Y.Y. Zhang, F. Wei, The road for nanomaterials industry: a review of carbon nanotube production, post-treatment, and bulk applications for composites and energy storage, Small 9 (2013) 1237–1265.
[49] H. Xie, R. Zhang, Y. Zhang, Z. Yin, M. Jian, F. Wei, Preloading catalysts in the reactor for repeated growth of horizontally aligned carbon nanotube arrays, Carbon 98 (2016) 157–161.
[50] E. Raymundo-Pinero, T. Cacciaguerra, P. Simon, F. Beguin, A single step process for the simultaneous purification and opening of multiwalled carbon nanotubes, Chem. Phys. Lett. 412 (2005) 184–189.
[51] B. Krause, M. Mende, P. Potschke, G. Petzold, Dispersability and particle size distribution of CNTs in an aqueous surfactant dispersion as a function of ultrasonic treatment time, Carbon 48 (2010) 2746–2754.
[52] N. Nair, W.-J. Kim, R.D. Braatz, M.S. Strano, Dynamics of surfactant-suspended single-walled carbon nanotubes in a centrifugal field, Langmuir 24 (2008) 1790–1795.
[53] F. Avilés, J. Cauich-Rodríguez, L. Moo-Tah, A. May-Pat, R. Vargas-Coronado, Evaluation of mild acid oxidation treatments for MWCNT functionalization, Carbon 47 (2009) 2970–2975.
[54] J.N. Israelachvili, Intermolecular and Surface Forces: Revised Third Edition, Academic press, 2011.
[55] K. Kordás, T. Mustonen, G. Tóth, H. Jantunen, M. Lajunen, C. Soldano, S. Talapatra, S. Kar, R. Vajtai, P.M. Ajayan, Inkjet printing of electrically conductive patterns of carbon nanotubes, Small 2 (2006) 1021–1025.
[56] M.F. Islam, E. Rojas, D.M. Bergey, A.T. Johnson, A.G. Yodh, High weight fraction surfactant solubilization of single-wall carbon nanotubes in water, Nano Lett. 3 (2003) 269–273.
[57] C. Richard, F. Balavoine, P. Schultz, T.W. Ebbesen, C. Mioskowski, Supramolecular self-assembly of lipid derivatives on carbon nanotubes, Science 300 (2003) 775–778.
[58] G. Atesok, P. Somasundaran, L. Morgan, Adsorption properties of Ca2 + on Na-kaolinite and its effect on flocculation using polyacrylamides, Colloids Surf. 32 (1988) 127–138.
[59] T. Cosgrove, Colloid Science: Principles, Methods and Applications, John Wiley & Sons, 2010.
[60] V.S. Ramachandran, Concrete Admixtures Handbook: Properties, Science, and Technology, second ed. Noyes Publications, Park Ridge, N.J., U.S.A., 1995.